Vapor-liquid equilibria and mixture densities for 2,2,4,4,6,8,8-heptamethylnonane + N_2 and n-hexadecane + N_2 binary mixtures up to 535 K and 135 MPa

Aaron J. Rowane[a,b] *, Manolis Gavaises[a], Mark A. M[c]Hugh[c]

[a] Department of Mechanical Engineering and Aeronautics, City University of London, Northampton Square, ECIV 0HB London, UK

[b] Afton Chemical Limited, London Rd, Bracknell, RG12 2UW, Berkshire

[c] Department of Chemical and Life Science Engineering, Virginia Commonwealth University, 601 W Main St, Richmond, VA, 23284

Abstract

In this work, we report high-pressure, high-temperature (HPHT) mixture density and *T-p* isopleth (bubble (BP) and dew (DP) point) data for hexadecane (HXD) + N_2 and heptamethylnonane (HMN) + N_2 mixtures from ~323 to 523 K and pressures to ~100 MPa. Isothermal, mixture density data for both mixtures are measured in the single–phase region from the BP pressure to ~135 MPa and with ~ 14 to 90 mol% N_2. A HPHT variable-volume, windowed view cell is used for both density and phase behavior measurements using the synthetic method. Mixture densities are correlated with the modified Tait equation and isothermal BP/DP data are correlated with an Antoine-type equation to allow for reliable interpolation of the data sets. Mixture densities and BP/DP pressures are modeled with the PC-SAFT equation coupled with pure component parameters calculated with two different group contribution methods. Although fairly reasonable predictions of liquid mixture densities are obtained when the binary interaction

parameter, k_{ij}, is set to zero for both HXD + N_2 and HMN + N_2 mixtures, a value of k_{ij} equal to at least 0.119 is needed for both systems to obtain reasonable predictions of isothermal *p*-*x* behavior.

Key words: PC-SAFT, High Pressure, High Temperature, Bubble Points, Dew Points

1. Introduction

Accurate thermophysical fluid properties are crucial for the design and operation of chemical processes used to manufacture specialty chemicals, lubricants, crude oil, polymers, etc. [1, 2]. The need for a fluid property database is especially important when operating at high-pressure, high-temperature (HPHT) conditions, such as those encountered in the recovery of petroleum reserves in ultra-deep reservoirs, in the application of lubricants to reduce energy losses due to friction in the automotive and allied industries, and in the operation of highly efficient diesel engines designed to reduce soot emissions. The eventual depletion of fossil fuels and their negative environmental impact has led to exploration of sustainable energy sources offering reduced emissions. Alternative fuel sources that can be used as a direct replacement or blended with petroleum derived diesel to mitigate its use are advantageous as they do not require a complete overhaul of current automotive infrastructure. Biowaste derived, paraffinic diesels have been proposed as an alternative as they can be produced from nonedible components of food crops[3, 4], waste cooking oils[5], and slaughterhouse waste[6]. Paraffinic diesel fuels are produced by first, oxidizing the feedstock then converting it to middle distillate *n*-paraffins through Fisher-Tropsch (FT) synthesis. Finally, in a final step the mixture of *n*-paraffins is subjected to an isomerization hydrocracking process to convert a fraction of the fuel to *i*-paraffins[7]. The finished product is a

mixture of *n*-paraffins and *i*-paraffins where the ratio of the two chemical families and *i*-paraffins structure are dependent on the selectivity of the catalyst used and isomerization process conditions[8]. These considerations place a premium on the HPHT fluid properties of *i*-paraffins and *n*-paraffins and understanding how *i*-paraffin structure impacts their fluid properties. Several studies report phase behavior data for binary *n*-alkane + N_2 mixtures[9-13] , but only handful of studies report mixture densities for the *n*-alkane + N_2 systems[14-16]. However, to the best of our knowledge no data are available for middle distillate *i*-paraffins + N_2 mixtures.

Here we present experimental information on the mixture density and phase behavior of two C16 isomers, hexadecane (HXD) and heptamethylnonane (HMN), each with nitrogen (N_2). HXD and HMN are representative compounds from two prominent chemical families found in diesel fuels and, therefore, these two C16 isomers are often used as surrogates for diesel fuel[17]. In addition, fluid property studies incorporating surrogates HXD and HMN are also of significant industrial interests since they are reference fuels used to determine the cetane number of diesel fuel using ASTM D613[18]. The major components in air, N_2 and O_2, are both spherically symmetric diatomic gasses that exhibit similar intermolecular potentials. However, unlike O_2, N_2 is an inert gas which makes it a suitable surrogate for studies at HPHT conditions. This suggests the HPHT data obtained for HXD or HMN + N_2 mixtures can provide insight into the physical state of diesel fuel injected into an air environment prior to combustion in a diesel engine where concentrations of CO_2 and H_2O will be negligible

Currently, only two studies by Sultanov and coworkers[19] and Lin and coworkers[20] provide pressure-mole fraction (*p*-*x*) isothermal data for the HXD + N_2. Further only a single study by Zolghader et al.[16] reports mixture density data for the HXD + N2 system. Mixture density data obtained in the single-phase region are correlated using a modified Tait equation and isothermal

BP/DP data are correlated with an Antoine-type equation. Both correlations provide a facile means of interpolation of data needed for comparisons with available literature data. The HXD isothermal bubble (BP) and dew (DP) point data generated in this study are compared to *p-x* isotherms reported by Sultanov and coworkers[19] at temperatures from 323 to 523 K and to a single *p-x* isotherm at 426.7 K reported by Lin and coworkers[20]. Additionally, HXD saturated, liquid densities reported here are compared to those reported by Zolghader et al.[16]. To the best of our knowledge, there are no reported studies for HXD + N_2 mixture density data at pressures greater than saturation pressure. Furthermore, there are no phase behavior or mixture density data available in the literature for HMN + N_2 mixtures. Yang and coworkers[21] do report saturated, liquid densities for HXD + CO_2 mixtures and the trends observed in this study are contrasted with the trends for saturated, liquid densities found for both HXD + N_2 and HMN + N_2 mixtures.

The resultant mixture densities and phase behavior data are modeled using the Perturbed Chain Statistical Associating Fluid Theory (PC-SAFT) equation of state (EoS)[22] which has been shown to work considerably well for highly asymmetric mixtures of spherical and chain molecules. For example, García-Sánchez et al.[23] report PC-SAFT modeling results for various non-associating hydrocarbon + N_2 systems including the HXD + N_2 system. Here the pure component parameters used with the PC-SAFT EoS are calculated with the group contribution (GC) method of Sauer and coworkers[24] (S-GC) and the method of Tihic and coworkers[25] (T-GC). The differences between these two methods are that the S-GC parameters are regressed from a combined, normal and branched paraffin data set and the T-GC parameters are regressed from separate, normal and branched paraffin data sets. Tihic, et al. developed the GC method using both first-order (FOG) and second-order group (SOG) values for calculating pure-component parameters while Sauer and coworkers only use FOG.

2. Methods and Materials

2.1. Materials

Table 1 lists the source and mass fraction purity of each chemical used in this study, as received, in this study.

Table 1. Chemical samples used in this study listed with the source and mass fraction purity reported by the manufacturer.

Chemical Name	Source	Mass Fraction Purity	Analysis method[a]
n-Hexane	Sigma-Aldrich	≥ 0.990	GC
n-Hexadecane	Sigma-Aldrich	0.990	GC
2,2,4,4,6,8,8-Heptamethylnonane	Acros Organics	0.980	GC
Nitrogen	Air-Gas	1.000	

[a] Determined by gas chromatography (GC) by the supplier.

2.2. Methods

Figure 1 shows the variable-volume, view cell used for VLE and density measurements. Details on the experimental apparatus are found in previous publications[26-29] and here the main features of the apparatus are described. A screw-type, pressure generator (Model 37-5.75-60, High Pressure Equipment Co.) delivers or removes water to the back end of the cell and to a pressure gauge, used to measure pressures below ~65 MPa (Model CM57303, 0 - 68.9 MPa, standard uncertainty of 0.07 MPa, Heise Corporation), and to a transducer, used to measure pressures greater than ~65 MPa (Model 245BWGDNEAPW, 0 - 345 MPa, standard uncertainty of 0.34 MPa,

Viatran Corporation). Both the gauge and transducer are located external to the heated cell and maintained at ambient temperature. The system pressure is equal to the pressure of the water delivered to the cell plus/minus a correction of 0.07 MPa when moving the piston forward/back. The cell is wrapped with heating tape and then covered with insulation to generate the desired operating temperature maintained to within ± 0.2 K and measured with a type-K thermocouple (Omega Engineering) calibrated against an accurate RTD thermometer having certificate of calibration traceable to NIST standards (Model DURAC TP-R04, measurement range 173 to 673 K, permissible deviation of 0.06 K, H-B Instrument Company). The fluid of interest in the cell is mixed with a stir bar controlled by an external magnet/motor located underneath the cell. The contents of the cell are projected onto a video monitor using a camera (Model STC-N63CJ, Lenox Instrument Company) coupled to a borescope (Model HAWKEYE® Pro, Gradient Lens Corporation) placed against a cylindrical sapphire window (Hemlite sapphire, 1.905 cm thick x 1.905 cm outside diameter ± 0.005 cm, faces flat to 0.0008 cm and parallel to 0.0025 cm, and beveled edges 0.762 cm x 45°, GT Crystal Systems, LLC) sealed with an elastomeric o-ring.

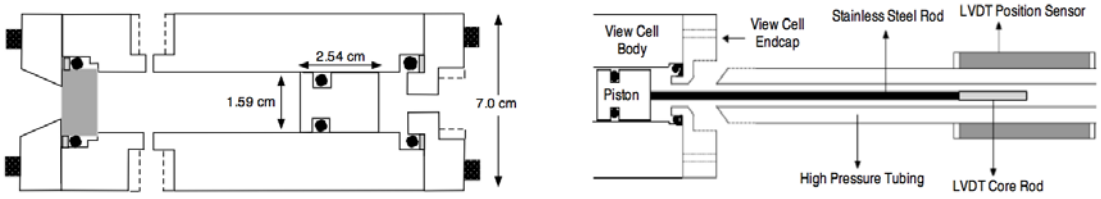

(A) (B)

Figure 1. Schematic diagram of (A) the high-presssure variable-volume, view cell and (B) the rod connecting the piston to the LVDT (not to scale).

For VLE and density measurements, the empty view cell is flushed three times with N_2 at ~2 MPa to reduce the residual air content to less than 10 ppm. After flushing, typically 0.025 g N_2 remains in the cell. Approximately 2.0 to 10.0 g of liquid HMN or HXD are charged to the cell using a syringe that is weighed (± 0.001 g) before and after loading. Next approximately 0.7 to 2.0 g of N_2 are loaded using a high-pressure, transfer vessel that is weighed (± 0.001 g) before and after loading. The final mass of N_2 in the cell includes any N_2 remaining in the cell at ambient pressure after flushing. The cell is then heated and pressurized to the desired temperature and pressure for VLE or density measurements.

2.2.1. VLE measurements

Once the desired temperature is reached, the mixture is stirred vigorously for 30 minutes to ensure thermal equilibrium. At a constant temperature, with a clear, single phase in the view cell, the system pressure is slowly reduced by ~0.5 MPa and the mixture again is stirred vigorously and allowed to come to thermal equilibrium. If a clear, single phase exists at this lower pressure, the system pressure is again slowly decreased by ~0.5 MPa and the mixture is again stirred vigorously and allowed to come to thermal equilibrium. This pressure reduction technique is continued until a small vapor bubble (bubble point, BP) appears for mixtures lean in N_2 or a mist or fog (dew point, DP) appears for mixtures very rich in N_2. The pressure is now increased well into the single-phase region and the solution is mixed to return to equilibrium. The pressure reduction technique is repeated with smaller step changes in pressure, several times, to reproduce the transition and to reduce the transition pressure. For both BP and DP measurements the composition of the predominant phase is considered equal to the overall solution composition since

the mass of the second phase is negligible. Data are obtained at pressures chosen in random order for a given isopleth to minimize any potential experimental artifacts in the measurements.

2.2.2. Density measurements

The internal cell volume is determined using a linear variable differential transformer (LVDT, Model 2000 HR, Measurement Specialties) that tracks a magnetic core at the end of a rod connected to the piston as shown in Figure 1. The piston position is correlated to the internal cell volume by calibration with hexane performed over the entire temperature-pressure range of interest in this study. Densimeter volume data are obtained at each temperature, pressure, and LVDT reading by dividing the known mass of hexane added to the cell with accurate hexane density data obtained from the NIST REFPROP program [30, 31]. Single-phase, mixture density data are calculated knowing the mass of solution loaded in the cell and the internal cell volume obtained from the LVDT calibration equation. Isothermal, mixture density data are recorded in the single–phase region from the BP pressure to ~135 MPa. For each isotherm, data are obtained at pressures chosen in random order to minimize any experimental artifacts in the measurements. The calculated maximum mole fraction expanded uncertainty is slightly more than 0.001 and the standard uncertainties of temperature and pressure are $u(T) = 0.2$ K and $u(p) = 0.07$ MPa for $p<68.9$ MPa and 0.34 MPa for $68.9<p<165$ MPa. The expanded accumulated uncertainty in the reported mixture densities is $U_c(\rho) = 0.80\%$ with a coverage factor, $k = 2$, which corresponds to a confidence interval of approximately 95%.

3. Experimental results

The SI provides p-T-x_{N2}-w_{N2} data tables for BP and DP transitions at given N_2 mole (x_{N2}) and weight (w_{N2}) fractions for both the HXD + N_2 mixtures and HMN + N_2 mixtures. Figure 2a shows p-T isopleths, that are transitions at constant composition, for HXD+ N_2 mixtures and Figure 2b shows similar isopleths for HMN + N_2 mixtures. Each isopleth shows the locus of BP or DP points that represent the transition from a single phase region at pressures above the curve to a two phase, liquid + vapor phase region at pressure below the curve. In this study we note that the gas solubility of N2 in both HXD + N_2 and HMN + N_2 mixtures increases with increasing temperature. This behavior is likely due to the increase in free volume of both C16 isomers with increasing temperature since intermolecular interactions between the mixture components are not expected to be strongly influenced by temperature for the same range of temperature increase[32].

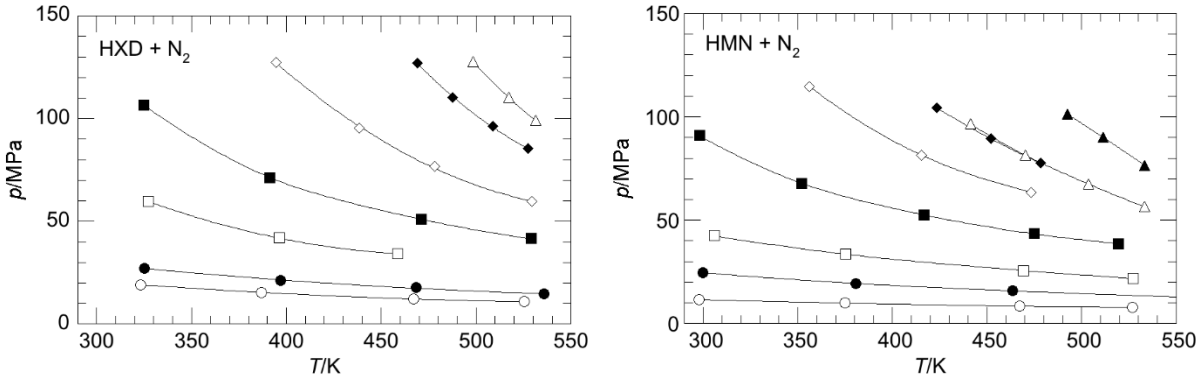

(a) (b)

Figure 2. Pressure-temperature isopleths obtained in this study for HXD + N_2 mixtures shown in (a) where ○ - 20.9, ● - 29.0, □ - 45.2, ■ - 58.1, ◇ - 68.5, ◆ - 81.6, and △ - 90.2 mol% N_2 and for HMN + N_2 mixtures shown in (b) where ○ - 14.9, ● - 29.0 (one data point is off the graph at 575.6 K), □ - 39.2, ■ - 57.1, ◇ - 67.1, ◆ - 76.0, △ - 77.3, ▲- 87.4 mol% N_2. Lines are drawn to guide the eye.

The SI provides p-T-x_{N2}-w_{N2} data tables for HXD + N_2 and HMN + N_2 mixture densities at a given x_{N2} and w_{N2}. The mixture density data obtained in this study are at x_{N2} from ~0.14 to 0.90, pressures to ~135 MPa, and temperatures to ~535 K. HXD + N_2 mixture density data are obtained at 26 isotherms (166 total points) held within ± 0.2 K except for the 527.0 K isotherm (± 0.8 K) and the 528.6 K isotherm (± 0.3 K). Likewise, HMN + N_2 mixture density data are obtained at 34 isotherms (166 total points) held within ± 0.2 K except for the 526.9 K isotherm (± 0.3 K) and the 528.0 K (± 0.5 K). Figure 3 shows an example of the effect of pressure and temperature on the density of HXD + N_2 and HMN + N_2 mixtures, each at slightly different, fixed mixture compositions and temperatures. Each density curve originates at the two-phase, BP boundary of the respective system and extends to ~120 MPa and temperatures from ~300 to 525 K. The density curves exhibit the expected trends with increasing temperature and pressure. The HXD + N_2 two-phase region in Figure 3(a) is expected to be smaller than that shown for the HMN + N_2 system since a higher amount of N_2 is dissolved in the HMN mixtures.

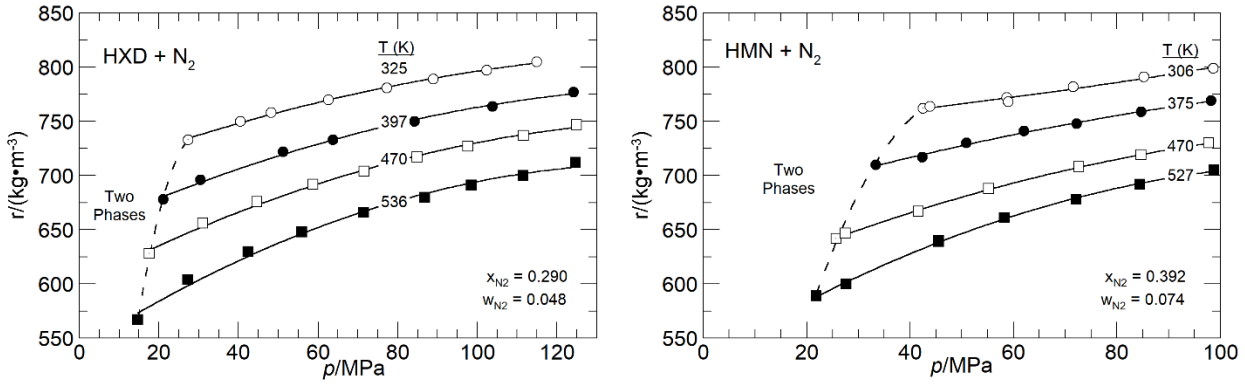

(a) (b)

Figure 3. Examples of experimental densities for HXD + N_2 mixtures (a) and HMN + N_2 mixtures (b) obtained in this study.

3.1 Correlation of experimental data

Correlation equations are used to facilitate interpolating pressure-composition (*p*-*x*) and density-composition (*ρ*-*x*) data and to generate plots of the data. Reliable correlations also serve as an effective means to compare previously reported phase behavior and mixture density data. In the present study BP and DP data are correlated with Antoine's equation and mixture density data are correlated with the Tait equation.

3.1.1 Correlation of BP data using Antoine's equation

Equation 1 shows Antoine's equation used for interpolation of the BP/DP data sets that allows for comparison of the results from the present study to any available literature. Values for parameters, *A*, *B*, and *C*, for both hydrocarbon + N_2 mixtures are obtained by minimizing the percent, average, absolute deviation (Δ_{AAD}, equation 2) for *p*-*T* data at each (HMN or HXD) + N_2 mixture composition. The SI provides tables reporting best-fit values for the parameters *A*, *B*, and *C* in equation 1 for both HXD + N_2 and HMN + N_2 along with Δ_{AAD} and the maximum deviation (Δ_{max}, equation 3) values. For 14 of the 15 data sets the fit of Antoine's equation agrees with experimental data resulting in Δ_{AAD} and Δ_{max} values that are less than or equal to 1%. One outlier is the HXD + N_2 data set at x_{N2} = 0.290 (Δ_{AAD} = 0.8% and Δ_{max} = 1.3%.)

$$ln\left(\frac{p}{MPa}\right) = A - \frac{B}{T+C} \quad (1)$$

$$\Delta_{AAD}/\% = 100 \cdot \frac{1}{N}\sum_{i=1}^{N}\left|\frac{x_{i,exp}-x_{i,cal}}{x_{i,exp}}\right| \quad (2)$$

$$\Delta_{max}/\% = Max\left(100 \cdot \left(\left|\frac{x_{i,exp} - x_{i,cal}}{x_{i,exp}}\right|\right)\right) \quad (3)$$

where $x_{i,exp}$ is an experimental point, $x_{i,cal}$ is a calculated point, and N is the number of data points.

Figure 4(a) shows select p-x_{N2} isotherms generated using the Antione's equation with parameters from the SI for the HXD + N_2 system and Figure 4(b) shows the expanded view of these isotherms using weight fraction rather than mole fraction. Figure 4(b) offers a clear picture of the experimental challenges measuring BP for these mixtures. These p-w_{N2} curves show that, on a mass basis, N_2 does not dissolve to a great extent in HXD even at temperatures as high as 423 K and elevated pressures, that is, these curves exhibit a very large positive slopes. Hence, a small error in N_2 mass loading can have a significant effect on measured BP values. In addition, the large positive slope in the p-w_{N2} curves are relatively insensitive to temperature variations at temperatures below 423 K and pressures to 100 MPa. Both the large positive slopes and lack of temperature sensitivity makes it challenging to precisely measure the BP for this sparingly soluble gas in HXD at these low temperature conditions. In contrast to this behavior, the location of the BP curves become more sensitive to pressure and temperature when operating from 473 to 523 K. Although the 523 K isotherm in Figure 4(b) is approaching a maximum, indicative of a mixture-critical point, we did not observe a mixture-critical point before reaching the T-p limit of our apparatus.

Figure 4(c) shows p-x_{N2} isotherms for the HMN + N_2 system at the same four temperatures as shown for the HXD + N_2 system in Figure 4(a). When comparing the isotherms in both figures it is apparent that N_2 more readily dissolves in HMN than HXD at a lower pressure, likely due to

the expected larger free volume of HMN, a highly branched hydrocarbon. At temperatures less than 423 K the HMN p-w_{N2} isotherms also exhibit fairly large positive slopes and the isotherms are very close to one another indicating a modest lack of temperature sensitivity. In contrast to the HXD system, BP and DP data are observed for the HMN system at N_2 loadings in excess of ~80 mol% (~30 mass%) at 473 and 523 K. Note that mixture-critical transitions were not clearly observed for any of the HMN measurements. Nevertheless, the 473 and 523 K isotherms are drawn as continuous curves with apparent mixture-critical points to connect the observed BP transitions to the DP transitions for mixtures. Note the very narrow width of the maxima at the two highest p-x_{N2} isotherms in Figure 4(c). This characteristic shape occurs for other binary mixtures containing compounds that have very large differences in molecular size and energetics.

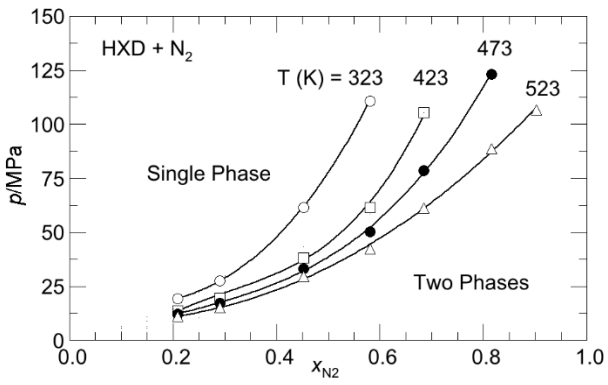

(a)

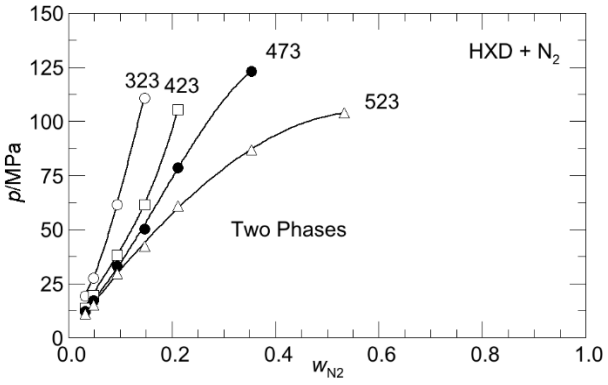

(b)

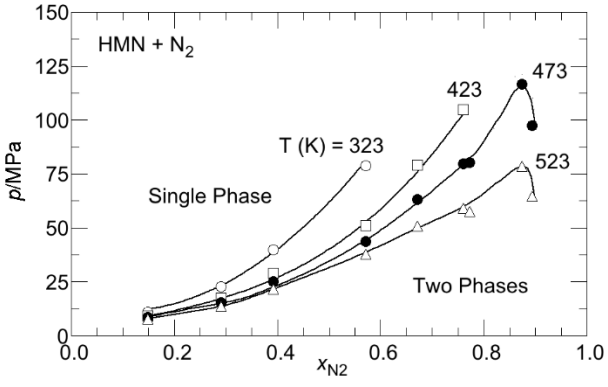

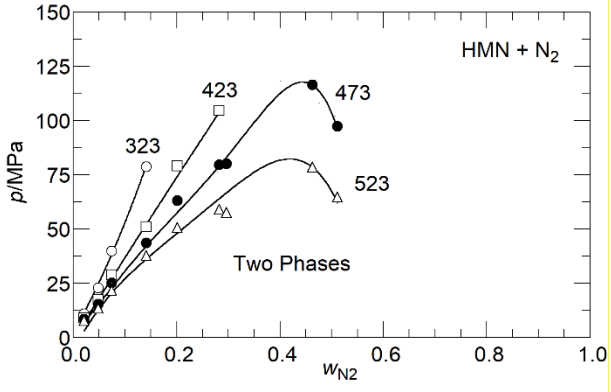

(c) (d)

Figure 4. P-x_{N2} and P-w_{N2} isotherms at 323, 423, 473, and 523 K for HXD + N_2 (a) and (b) and HMN + N_2 mixtures (c) and (d). Lines are drawn to guide the eye.

Figure 5a compares Antoine-calculated, HXD + N_2, BP data from the present study that overlaps with data to ~ 60 MPa reported by Sultanov et al.[19]. Only three out of five possible isotherms are shown in Figure 5a to avoid cluttering the graph. Similar trends for the shape and relative locations of the isotherm are observed in both studies. However, only the 323 and 523 K isotherms agree reasonably well with those of Sultanov and coworkers. The 423 K isotherm from the present study is shifted to higher N_2 mole fractions compared to Sultanov's data, as are isotherms at 373 and 473 K (not shown). It is worth noting that when we observed the lack of agreement for these isotherms, we recalibrated our pressure gauges and thermocouples, but found the T-p measurements to be reliable and accurate, as previously described in the experimental section. There appears to be no apparent reason for the discrepancies with the "middle" temperature isotherms reported by Sultanov and coworkers[19].

Figure 5b shows reasonable agreement between the Antoine-calculated, HXD + N_2, BP data from the present study with the data at 462.7 K reported by Lin et al.[20]. Unfortunately, the 462.7 K isotherm is the only one that partially overlaps with conditions of the present study. It is worth noting that Lin and coworkers performed measurements with a dynamic flow technique at extreme temperatures of 463 to 703 K[33], but only to pressures of ~ 25 MPa. In contrast, the synthetic method is used in the present study to measure BP data to temperatures of ~ 525 K and pressures to at least 100 MPa. The advantage with the synthetic technique used here is that it is

also possible to obtain reliable mixture density data at constant composition and temperature starting at the BP and operating to much higher pressures.

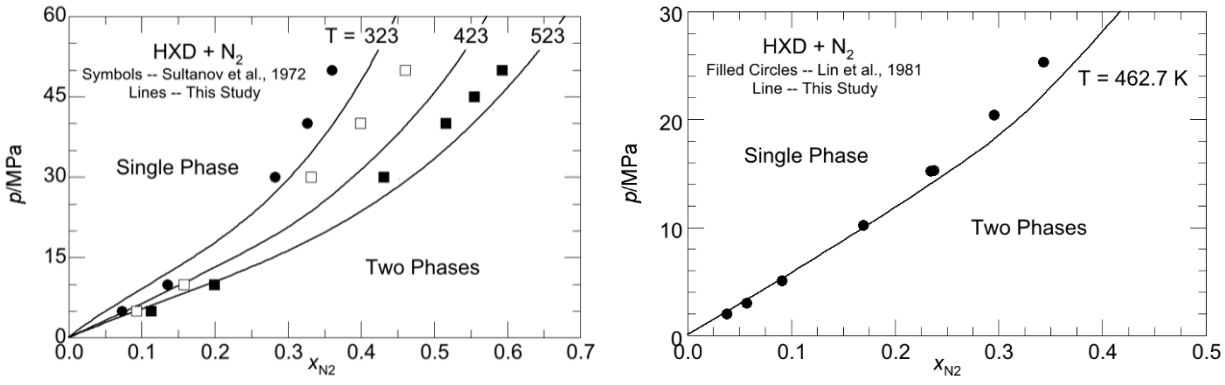

(a) (b)

Figure 5. Comparison of BP data calculated using Antoine's equation fit to HXD +N_2 data obtained in the present study (lines) to data of Sultanov et al.[19] shown in (a) at ● - 323, ○ - 423, and ■ - 523 K and to data of Lin et al. shown in (b) at ● - 462.7 K.

3.1.2 Correlation of density data using the Tait equation

Mixture density data obtained in the single-phase region are correlated using the Tait equation given by equations 4 to 6. Unlike in previous studies where the Tait reference density, $\rho_0(T)$, is calculated at p_0 = 0.1 MPa, here p_0 is set equal to the BP or DP pressure at each T-x_{N2} condition calculated with Antoine's equation and best-fit parameters. Each mixture density, isothermal, isopleth is first fit to the Tait equation by varying C, $\rho_0(T)$, and $B(T)$ to minimize the Δ_{AAD} and constraining the bias (Δ_{bias}, equation 7) to zero. Once values of $\rho_0(T)$ and $B(T)$ are determined at each temperature these parameters are then fit to polynomials of temperature given by equations 5 and 6. Finally, the parameters C, a_0, a_1, a_2, b_0, b_1, and b_2 are refit simultaneously to all of the mixture density, isothermal isopleths by minimizing Δ_{AAD} and constraining Δ_{bias} to zero.

The SI provides tables listing the parameters used with equations 4 to 6 for both HMN or HXD + N_2 mixtures at each mixture composition where parameters for pure HMN or HXD are from our previous study[34]. With this calculation scheme the Δ_{AAD} varies from 0.1 to 0.3% and Δ_{MAX} varies from 0.2 to 1.2% at temperatures from 298 to 533 K and pressures from 4 to 135 MPa.

$$\frac{\rho-\rho_0(T)}{\rho} = C \log_{10}\left(\frac{P+B(T)}{P_0+B(T)}\right) \quad (4)$$

$$\rho_0(T)/kg \bullet m^{-3} = \sum_{i=0}^{2} a_i T^i \quad (5)$$

$$B(\mathrm{T})/MPa = \sum_{i=0}^{2} b_i T^i \quad (6)$$

$$\Delta_{bias}/\% = \frac{1}{N}\sum_{i=1}^{N} 100 \cdot \left(\frac{x_{i,exp}-x_{i,cal}}{x_{i,exp}}\right) \quad (7)$$

The Tait equation, with parameters found in the SI, is used to create Figures 6a and 6b that shows the variation of the saturated, liquid-phase mixture density as N_2 dissolves in HMN or HXD at a fixed temperature and, implicitly, as a function of pressure. Here we compare the trends for HXD + N_2 mixture densities with the trends reported by Yang et al.[21] for saturated liquid densities for HXD + CO_2 mixtures. Yang and coworkers show that the dissolution of CO_2 into HXD increases mixture densities at low temperatures and decreases mixture densities at high temperatures. However, this study is limited to a maximum temperature of 473 K and a maximum pressure of 50 MPa where CO_2 can still be considered a compressed, dense gas not far it's critical point. In contrast, N_2 is an expanded supercritical fluid at temperatures from 300 to 525 K, which

is two to four times higher than the critical temperature of N_2 (~126 K). Figure 6a shows that HXD + N_2 mixture densities initially decrease as N_2 dissolves into HXD at all temperatures from 323 to 525 K. However, the mixture densities exhibit a shallow minimum with respect to increasing N_2 mole fraction at ~ 0.35. At higher N_2 mole fractions, mixture densities now increases as more N_2 dissolves in the mixture. This minimum in the saturated density curve is especially prominent for the 323 K isotherm in Figure 6a. The shape of the ρ-x_{N2} curves reflect a balance between the reduction in liquid mixture density as N_2 dissolves into HXD and the increase in liquid mixture density as the system pressure is increased to force N_2 into the HXD. This conflict of effects is exacerbated at the lowest temperatures where N_2 is only sparingly soluble in HXD as reflected in the almost vertical BP isotherms shown in Figure 3b. At operating temperatures of ~ 473 K and higher, the pressure effect is a bit less pronounced since an increased amount of N_2 can more easily dissolve in the thermally-expanded HXD. Ultimately, at 523 K, the highest temperature shown in Figure 6a, the ρ-x_{N2} curve exhibits a very small maximum since the densities now have greater than 80 mol% N_2.

Figure 6b shows the impact of N_2 solubility and pressure on the saturation density curves for HMN + N_2 mixtures. Many of the same composition and pressure trends are observed with the HMN system as observed with the HXD system. However, in this instance the pronounced minimum in the ρ-x_{N2} curve is diminished at a lower temperature of ~ 423 K, the density curve at 473 exhibits a modest negative slope, and the 523 K turns to lower densities near ~ 0.8 since the last data point in this figure represent a DP not a BP.

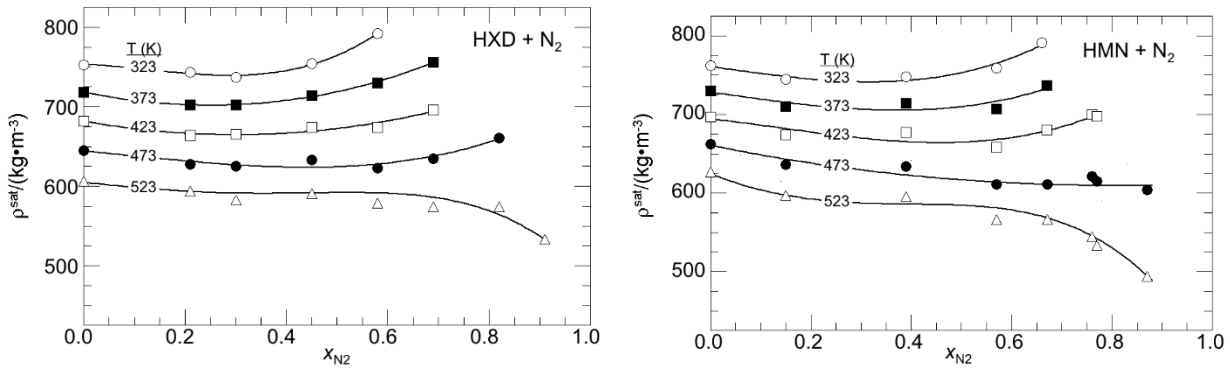

(a) (b)

Figure 6. The relationship between Tait-calculated, saturated liquid densities and N_2 mole fraction in (a) HXD + N_2 mixtures and in (b) HMN + N_2 mixtures obtained in the present study. ○ - 323, ■ - 373, □ - 423, ● - 473, and △ - 523 K.

Zolghadr et al.[16] report saturated liquid mixture densities for the HXD + N_2 system at temperatures from 313 to 393 K and pressures to ~ 42 MPa. However, the authors of this study only provide a very meager amount of experimental detail for these density measurements. For example, the authors do not offer verification that a single phase exists in the densimeter, they do not report whether the HXD + N_2 mixtures were well mixed and maintained at saturation conditions, and they do not report the equilibrium concentration of N_2 at *T-p* conditions. Nevertheless, Figure 7 shows a deviation plot comparing Tait-calculated, saturated liquid densities for HXD + N_2 mixtures from the present study to saturated liquid densities reported by Zolghadr et al.[16] The densities at 333 K agree within the estimated uncertainty of the present study over the entire pressure range reported by Zolghadr and coworkers. However, the saturated liquid mixture densities reported by Zolghadr and coworkers at 353, 373, and 393 K differ by more than 1% from those in the present study.

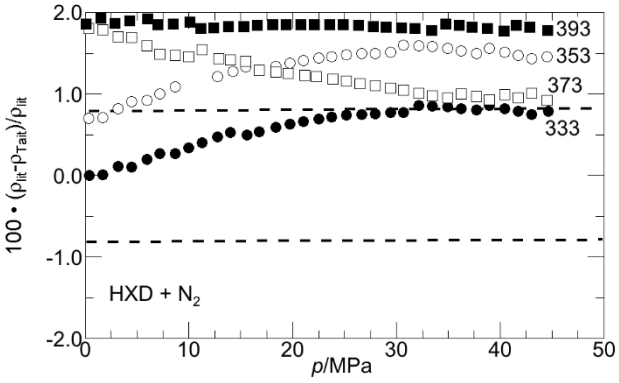

Figure 7. Comparison of saturated liquid mixture densities reported by Zolghadr et al.[16], ρ_{lit}, to Tait-calculated densities from the present study, ρ_{Tait}, as a function of pressure up to ~ 42 MPa. ● - 333, ○ - 353, □ - 373, and ■ - 393 K. Lines are drawn at ± 0.8% representing the combined expanded estimated uncertainty of the densities reported in this study.

3.1.3 Modeling experimental data using the PC-SAFT EoS

The PC-SAFT EoS is described in general terms here and the reader is directed to the literature for more details [22]. The EoS is derived from the residual, reduced Helmholtz free energy, a^{res},

$$a^{res} = a^{hc} + a^{disp} + a^{assoc} \quad (8)$$

where a^{hc} is the hard chain fluid contribution, a^{disp} is the dispersion interaction contributions, and a^{assoc} is the contribution from self- and cross-association complex formation, which is not applicable here since HXD and HMN do not self- or cross-associate with N_2. The approach taken

in the present study is to assess the performance of the PC-SAFT EoS using two different group contribution (GC) methods to calculate the three, pure-component parameters *m*, σ, ε/k for HXD and HMN. One approach is the GC method of Sauer et al.[24] (S-GC) with parameters regressed from a combined, normal and branched paraffin data set. The other approach is the GC method of Tihic et al.[25] (T-GC) with parameters regressed from separate, normal and branched paraffin data sets. Tihic developed the GC method using both first-order (FOG) and second-order group (SOG) values for calculating pure-component parameters while Sauer only use FOG. Table 2 lists calculated values for *m*, *σ*, and *ε*/*k* for HXD and HMN obtained with both approaches. Parameters for N_2, determined from a fit of the EoS to the N_2 vapor pressure curve and saturated liquid densities, are taken directly from the literature[22].

Table 2. PC-SAFT EoS parameters *m*, *σ*, and *ε*/*k* calculated using Tihic's and Sauer's GC methods for both HXD and HMN. Parameters for N_2 are taken directly from the literature.[22]

HXD

	m	σ/Å	ε/k/K
Sauer et al.[24]	7.609	3.8637	237.54
Tihic et al.[25]	6.669	3.9440	253.59

HMN

Sauer et al. [24]	5.009	4.2774	284.79
Tihic et al.[25]	5.603	4.1640	266.46

N_2

Gross and Sadowski[22]	1.205	3.313	90.96

Equations 14-16 show the combining rules used to calculate m for a mixture and the cross terms, σ_{ij} and ε_{ij}, needed for mixture calculations with the PC-SAFT EoS as described by Gross and Sadowski[22]. Here HPHT mixture density data are compared to purely predictive model calculations with k_{ij} set to zero for both GC methods since interaction energies are less sensitive than m and σ to variations in density. Subsequently BP/DP behavior are modeled with both zero and non-zero values for k_{ij} using both GC methods since phase behavior calculations are very sensitive to variations in ε. The performance of the PC-SAFT EoS in each case is characterized by the resultant values for the Δ_{AAD} , Δ_{stdev}, Δ_{bias}, and Δ_{max}. The calculations are performed using commerically available software, VLXE[35].

$$m = \sum_i x_i m_i \tag{14}$$

where x_i is the mole fraction of component i.

$$\sigma_{ij} = 0.5(\sigma_i + \sigma_j) \tag{15}$$

$$\varepsilon_{ij} = (1 - k_{ij})\sqrt{\varepsilon_i \varepsilon_j} \tag{16}$$

3.1.4 Modeling mixture densities

Figure 8 illustrates the performance of the PC-SAFT EoS for density predictions using either the S-GC or T-GC parameters listed in table 2 for both HXD + N_2 and HMN +N_2 mixtures and with $k_{ij} = 0$ for all cases. Figure 8 shows the same Δ_{AAD} value is obtained for the HXD + N_2 system regardless which parameter set is used. However, figure 8 also shows a significantly better

Δ_{AAD} value for HMN + N_2 mixtures using T-GC parameters as compared to S-GC parameters. A likely reason for the better performance of the T-GC method is that Tihic and coworkers regressed GC parameters from independent sets of normal and branched alkane data whereas Sauer and coworkers grouped normal and branched alkane data sets. Additional statistical performance measures are provided in the supplemental information for density predictions using the two different GC methods.

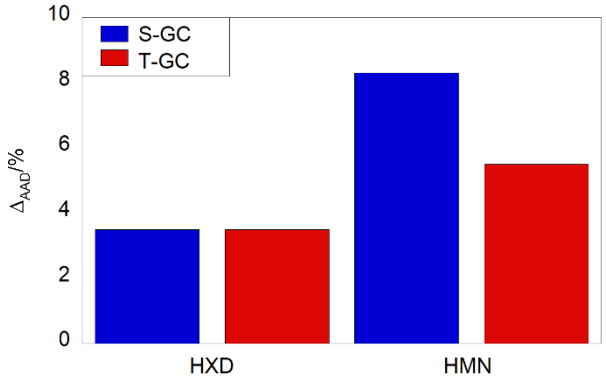

Figure 8. Performance of the PC-SAFT EoS for density predictions using the group contribution method of Sauer et al. (S-GC) and Tihic et al. (T-GC) with k_{ij} = 0 for all cases.

3.1.5 Modeling VLE

Figures 9a and 9b illustrate the performance of the PC-SAFT EoS for HXD + N_2 and HMN + N_2 BP/DP predictions using parameters calculated with the two GC methods when k_{ij} = 0 and when the best-fit k_{ij} is used, respectively. Table 3 provides the best-fit k_{ij} values for both the HXD + N_2 and HMN + N_2 systems when using either S-GC or T-GC parameters. As shown in figure 9a the resultant Δ_{AAD} values are insensitive to the choice of GC parameters. Additionally, it is worth noting that BP/DP predictions are grossly underpredicted when k_{ij} = 0 in all cases for the systems studied here (see additional statistical measures of the EoS performance listed in the SI). Figure

9b shows that Δ_{AAD} is about a factor of two lower for the HXD + N_2 system when using T-GC parameters. However, the choice of GC parameters has no impact on the Δ_{AAD} values for the HMN + N_2 system. It is not apparent why a non-zero kij has a noticeably different impact on the VLE predictions for the HXD system as compared to the HMN system. Given that a non-zero value only corrects the energetic parameter in the PC-SAFT EoS, it is possible that the difference in performance of the EoS for both systems is a result of the very different values for the other two EoS parameters, m and sigma, calculated with both GC methods. Further, in depth, parametric studies are needed to resolve this observed difference in performance of the GC methods with the PC-SAFT EoS.

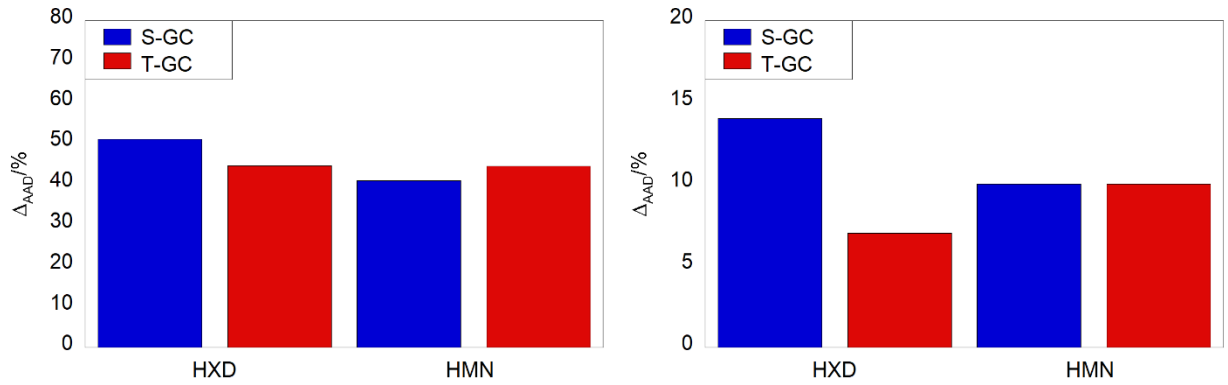

(a) (b)

Figure 9. Performance of the PC-SAFT EoS for VLE predictions using the group contribution methods of Sauer et al. (S-GC) and Tihic et al. (T-GC). (a) k_{ij} = 0 is used and (b) best-fit values for k_{ij} are used. In this case Δ_{AAD} compares experimental and calculated BP/DP pressures.

Table 3. Best-fit k_{ij} values for HXD + N_2 and HMN + N_2 mixtures using parameters calculated using either the group contribution method of Sauer et al. (S-GC) or Tihic et al. (T-GC).

	k_{ij}	
	S-GC	T-GC
HXD	0.134	0.119
HMN	0.125	0.130

Figures 10(a) and 10(b) show comparisons of experimental and calculated isotherms for HXD + N_2 and HMN + N_2 mixtures, respectively, using pure component parameters calculated with the T-GC method. Figure 10(a) shows a good fit for the 323 to 423 K isotherms with only a modest fit of the 530 K isotherm. In fact, with k_{ij} = 0.119 the predicted mixture-critical point at 523 K and ~115 MPa is not observed experimentally, as shown in Figure 4(a). Garcia-Sanchez and coworkers[23] also find it necessary to increase the value of k_{ij} to expand the two-phase region and increase the mixture-critical pressure. Figure 10(b) shows the same calculated trends with the HMN + N_2 system as seen for the HXD + N_2 system. For the HMN + N_2 system the p-x_{N2} isotherms at 323 to 423 K are fit well with k_{ij} = 0.130; however, the mixture-critical point is predicted to be well in excess of 125 MPa whereas the data in Figure 3c suggest this point should be at slightly less than 125 MPa. In contrast, the predictions for the 530 K isotherm are reasonably close to the actual observed behavior. Although not shown here, the same calculated trends are seen for both mixtures when using S-GC parameters.

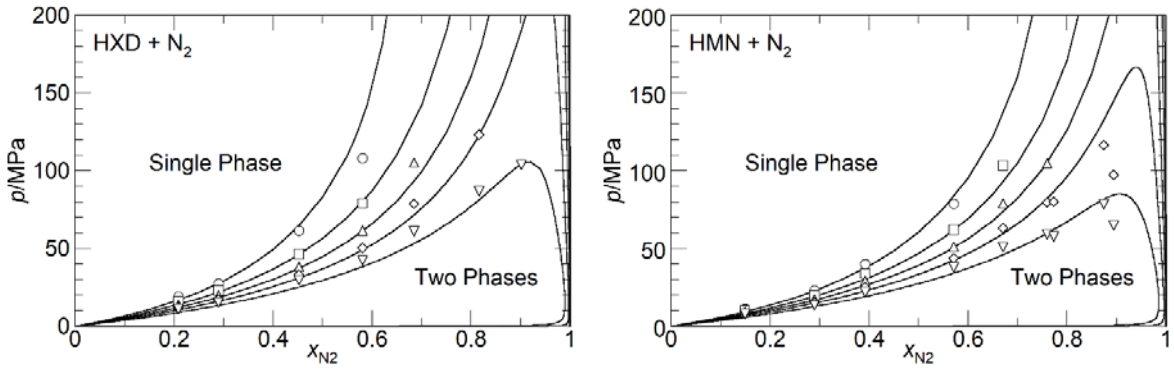

(a) (b)

Figure 10. Comparison of experimental (symbols) and PC-SAFT calculated (lines) isotherms with pure component parameters calculated with the T-GC method for (a) HXD + N_2 mixtures with k_{ij} = 0.119, and (b) HMN + N_2 mixtures with k_{ij} = 0.130. ○ - 323, □ - 373, △ - 423, ◇- 473, and ▽ - 530 K.

Figures 11(a) and 11(b) show predicted mixture critical curves for the HXD + N_2 and HMN + N_2 systems when using the best fit k_{ij} values with the S-GC and T-GC parameters, respectfully. In both instances the predicted mixture-critical curves exhibit type III behavior[36], which is representative of binary mixtures with molecular components that have very different molecular sizes and energetics. Figure 11(a) shows the predicted mixture-critical curves for the HXD + N_2 and HMN + N_2 systems using the best-fit k_{ij} values and S-GC parameters. Two solid line representing pure component vapor pressure curves for HXD and HMN essentially superpose in the *p*-*T* diagram. Predicted pure component critical points for HXD and HMN are ~710 and ~755 K, respectfully, which differ from the reported values of 722 K and 1.4 MPa for HXD[37] and 692 K and 1.57 MPa for HMN[38]. Additionally, predictions with the PC-SAFT when using the S-GC parameters provide the incorrect trend predicting both greater mixture critical points for HMN +

N_2 and greater a pure component critical point for HMN than HXD + N_2 and HXD, respectfully. Figure 11(b) shows the predicted mixture-critical curves for the HXD + N_2 and HMN + N_2 systems using the best fit k_{ij} values and T-GC parameters. In this instance the calculated critical points for HMN and HXD are quite close to one another at ~734 K and 1.7 MPa which still differs from reported values. However, predicted mixture critical points for HMN + N_2 are lower than that of HXD + N_2 at which is what is shown experimentally. The better representation of the PC-SAFT EoS when using the T-GC parameters may due to the inclusion of SOG which are not included in the S-GC database.

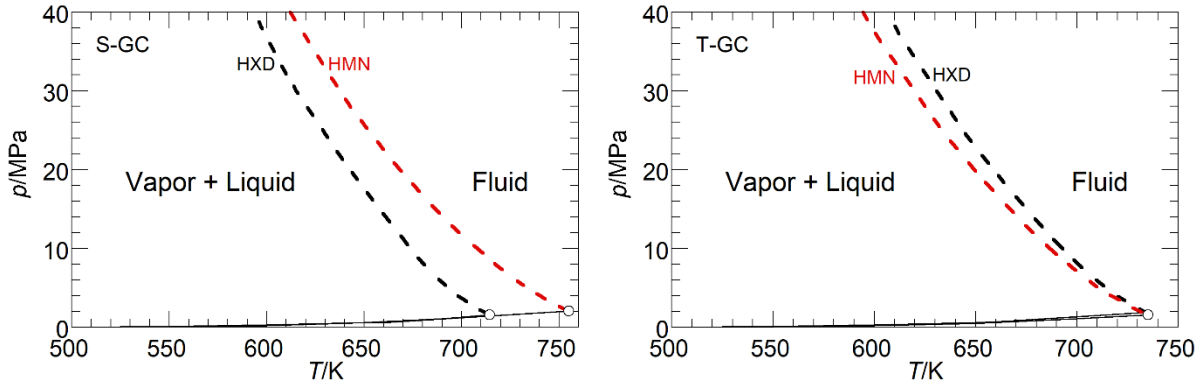

(a) (b)

Figure 11. PC-SAFT calculated *p-T* diagram for HXD + N_2 and HMN + N_2 mixtures where (a) using pure component parameters calculated using GC method of (a) Sauer et al. and (b) Tihic et al. In both cases the calculated vapor pressure curves for HXD and HMN (solid lines) essentially superpose each ending at the predicted pure component critical point (open circle). The HMN + N_2 mixture-critical curve (red dashed line) the HXD + N_2 mixture-critical curve (black dashed line) are calculated with the best fit k_{ij} values.

4.Conclusions

Mixture densities and bubble and dew point data are reported at temperatures to ~525 K and pressures up to ~125 MPa for C16 isomers, HXD or HMN, in N_2. The reported mixture density data are valuable to quantitatively assess the effect of molecular structure on HPHT fluid properties and to add to the existing property database for these two isomers. The data are also of value since these C16 isomers are often used as surrogates for diesel fuel, a complex multicomponent mixture. The experimental data are modeled using the PC-SAFT EoS with Sauer's and Tihic's GC methods to calculate pure component parameters that allow for density and phase behavior predictions. Mixture densities are predicted almost equally well with parameters from either GC method with the binary interaction coefficient set equal to zero. This result is not surprising since mixture density data do not offer a very sensitive test for the performance of an EoS. However, very poor predictions of the phase behavior of both HXD or HMN + N_2 mixtures are obtained, regardless of which GC method is used, if the binary interaction parameter is set to zero. Although it is difficult to get an accurate fit of all of the observed isotherms using a nonzero, positive value for k_{ij} with either GC method for both mixtures, it is worth noting that the data span a 200 K range which suggests that k_{ij} may need to be a function of temperature. In addition, the model calculations presented in this study clearly show the sensitivity of the results to the EoS pure component parameters obtained with two different group contribution methods. For these C16-N_2 mixtures, PC-SAFT calculations with T-GC parameters appear to provide more reasonable predictions of the phase behavior extrapolated to very high temperatures as compared to calculations using S-GC parameters. This result is directly related to the method used to generate GC parameters.

Acknowledgments

This project has received funding from the European Union Horizon 2020 Research and Innovation program, Grant Agreement No 675528. The authors thank Joseph Roos (Afton), Joseph Remias (Afton), Joshua Moore (Afton), Ashu Gupta (Afton), and Mark Devlin (Afton) for their helpful, technical insight with this study.

References

1. Gupta, S.; Olson, J. D., Industrial Needs in Physical Properties. *Ind Eng Chem Res* **2003,** 42, 6359-6374.
2. Hendriks, E.; Kontogeorgis, G. M.; Dohrn, R.; de Hemptinne, J.-C.; Economou, I. G.; Žilnik, L. F.; Vesovic, V., Industrial Requirements for Thermodynamics and Transport Properties. *Ind Eng Chem Res* **2010,** 49, 11131-11141.
3. Hamelinck, C. N.; Faaij, A. P. C.; den Uil, H.; Boerrigter, H., Production of FT transportation fuels from biomass; technical options, process analysis and optimization, and development potential. *Energy* **2004,** 29, 1743-1771.
4. Zwart, R. W. R.; Boerrigter, H., High efficiency co-production of synthetic natural gas (SNG) and fisher-tropsch (FT) transportation fuels from biomass. *Energy Fuels* **2005,** 19, 591-597.
5. Srivastava, S. P.; Hancsók, J., *Fuels and Fuel-Additives*. 1st ed.; John Wiley & Sons, Inc.: Hoboken, New Jersey, 2014; p 364.
6. Zahos-Siagos, I.; Karonis, D., Exhaust emissions and physiochemical properties of hydrotreated used cooking oils in blends with diesel fuel. *Int J Chem Eng* **2018,** 2018, 1-10.

7. Brownstein, A. M., *Renewable Motor Fuels*. Butterworth-Heinemann: 2015; p 134.
8. Deldari, H., Suitable catalysts for hydroisomerization of long-chain normal paraffins. *Appl Catal, A* **2005,** 293, 1-10.
9. García-Córdova, T.; Justo-Garcíam, D. N.; García-Flores, B. E.; García-Sánchez, F., Vapor-liquid equilbrium data for the nitrogen+ dodecane system at temperatures from (344 to 593) K and at pressures up to 60 MPa. *J Chem Eng Data* **2011,** 56, 1555-1564.
10. García-Sánchez, F.; Eliosa-Jiménez, G.; Silva-Oliver, G.; García-Flores, B. E., Vapor-liquid equilibrium data for the nitrogen + *n*-decane system from (344 to 563) K and at pressures up to 50 MPa. *J Chem Eng Data* **2009,** 54, 1560-1568.
11. García-Sánchez, F.; Eliosa-Jiménez, G.; Silva-Oliver, G.; Godínez-Silva, A., High-pressure (vapor + liquid) equilibria in the (nitrogen + n-heptane) system. *J Chem Thermodynam* **2007,** 39, 893-905.
12. Tong, J.; Gao, W.; Robinson, R. L.; Gasem, K. A. M., Solubilities of Nitrogen in Heavy Normal Paraffins from 323 to 423 K at Pressures to 18.0 MPa. *J Chem Eng Data* **1999,** 44, 784-787.
13. Uribe-Vargas, V.; Trejo, A., Vapor–liquid equilibrium of nitrogen in an equimolar hexane + decane mixture at temperatures of 258, 273, and 298 K and pressures to 20 MPa. *Fluid Phase Equilib* **2004,** 220, 137-145.
14. Jianhua, T.; Satherley, J.; Schiffrin, D. J., Density and interfacial tension of nitrogen-hydrocarbon systems at elevated pressures. *Chin J Chem Eng* **1993,** 1, 223-231.
15. Pereira, L. M. C.; Chapoy, A.; Burgass, R.; Tohidi, B., Measurement and modelling of high pressure density and interfacial tension of (gas + *n*-alkane) binary mixtures. *J Chem Thermodyn* **2016,** 97, 55-69.

16. Zolghadr, A.; Riazi, M.; Escrochi, M.; Ayatollahi, S., Investigating the effects of temperature, pressure, and paraffin groups on the N_2 miscibility in hydrocarbon liquids using the interfacial tension measurement method. *Ind Eng Chem Res* **2013,** 52, 9851-9857.
17. Mueller, C. J.; Cannella, W. J.; Bays, J. T.; Bruno, T. J.; DeFabio, K.; Dettman, H. D.; Gieleciak, R. M.; Huber, M. L.; Kweon, C.-B.; McConnell, S. S.; Pitz, W. J.; Ratcliff, M. A., Diesel surrogate fuels for engine testing and chemical-kinetic modeling: Compositions and properties. *Energy Fuels* **2016,** 30, 1445-1461.
18. *ASTM D613 - 18a, Standard test method for cetane number of diesel fuel oil*. ASTM International: West Conshohocken, PA, 2018.
19. Sultanov, R. G.; Skripka, V. G.; Namiot, A. Y., Phase Equilibrium of Methane and Nitrogen with High-Boiling Hydrocarbons. *Gasov Delo* **1972,** 10, 43-46.
20. Lin, H.-M.; Kim, H.; Chao, K.-C., Gas-liquid equilibria in nitrogen + *n*-hexadecane mixtures at elevated temperatures and pressures. *Fluid Phase Equilib* **1981,** 7, 181-185.
21. Yang, P.; Guo, H.; Wang, Z.; Zhou, Q., Density and volumetric properties of binary mixtures of CO_2 + hexadecane from (303.2 to 473.2) K and pressures up to 50 MPa. *J Chem Eng Data* **2019,** In Press.
22. Gross, J.; Sadowski, G., Perturbed-Chain SAFT: An Equation of State Based on a Perturbation Theory for Chain Molecules. *Ind Eng Chem Res* **2001,** 40, 1244-1260.
23. García-Sánchez, F.; Eliosa-Jiménez, G.; Silva-Oliver, G.; Vázquez-Román, R., Vapor–liquid equilibria of nitrogen–hydrocarbon systems using the PC-SAFT equation of state. *Fluid Phase Equilib* **2004,** 217, 241-253.

24. Sauer, E.; Stavrou, M.; Gross, J., Comparison between a homo- and a heterosegmented group contribution approach based on the perturbed-chain polar statistical associating fluid theory equation of state. *Ind Eng Chem Res* **2014,** 53, 14854-14864.
25. Tihic, A.; Kontogeorgis, G. M.; von Solms, N.; Michelsen, M. L., A predictive group-contribution simplified PC-SAFT equation of state: Application to polymer systems. *Ind Eng Chem Res* **2008,** 47, 5092-5101.
26. Liu, J.; Kim, Y.; M^{c}Hugh, M. A., Phase behavior of diisobutyl adipate-carbon dioxide mixtures. *Fluid Phase Equilib* **2006,** 248, 44-49.
27. Liu, K.; Wu, Y.; M^{c}Hugh, M. A.; Baled, H.; Enick, R. M.; Morreale, B. D., Equation of state modeling of high-pressure, high-temperature hydrocarbon density data. *J Supercrit Fluids* **2010,** 55, 701-711.
28. Mallepally, R. R.; Gadepalli, V. S.; Bamgbade, B. A.; Cain, N.; M^{c}Hugh, M. A., Phase behavior and densities of propylene + hexane binary mixtures to 585 K and 70 MPa. *J Chem Eng Data* **2016,** 61, 2818-2827.
29. Wu, Y.; Bamgbade, B. A.; Liu, K.; M^{c}Hugh, M. A.; Baled, H.; Enick, R. M.; Burgess, W. A.; Tapriyal, D.; Morreale, B. D., Experimental measurements and equation of state modeling of liquid densities for long-Chain *n*-alkanes at pressures to 265 MPa and temperatures to 523 K. *Fluid Phase Equilib* **2011,** 311, 17-24.
30. Lemmon, E. W.; Huber, M. L.; McLinden, M. O., REFPROP 9.1. **2013,** 23.
31. Lemmon, E. W.; Span, R., Short fundemental equations of state for 20 industrial fluids. *J Chem Eng Data* **2006,** 51, 785-850.
32. Prausnitz, J. M.; Lichtenthaler, R. N.; Gomes de Azevedo, E., *Molecular Thermodynamics of Fluid-Phase Equilibria*. Prentence Hall: 1999; p 860.

33. Simnick, J. J.; Lawson, C. C.; Lin, H.-M.; Chao, K.-C., Vapor-liquid equilibrium of hydrogen/tetraIin system at elevated temperatures and pressures. *AIChE J* **1977,** 23, 469-476.

34. Rowane, A. J.; Mallepally, R. R.; Gupta, A.; Gavaises, M.; M^{c}Hugh, M. A., High-temperatures, high-pressure viscosities and densities of *n*-hexadecane, 2,2,4,4,6,8,8-heptamethylnonane, and squalane measured using a universal calibration for a rolling-ball viscometer/densimeter. *Ind Eng Chem Res* **2019,** 58, 4303-4316.

35. Laursen, T. VLXE, V. 9.3. www.vlxe.com

36. Scott, R. L.; van Konynenburg, P. H., Static properties of solutions. Van der Waals and related models for hydrocarbon mixtures. *Discuss Faraday Soc* **1970,** 49, 87.

37. Ambrose, D.; Tsonopoulos, C., Vapor-liquid critical properties of elements and componds. 2. Normal alkenes. *J Chem Eng Data* **1995,** 40, 531-546.

38. Ambrose, D.; Ghiassee, N. B., Vapor pressure and critical temperature and critical pressure of 2,2,4,4,6,8,8-heptamethylnonane. *J Chem Thermodyn* **1988,** 20, 1231-1232.